University of Reading

Quantifying sources of inter-model diversity in the cloud albedo effect

Article

Supplemental Material

Online Open

Wilcox, L. J. ORCID: https://orcid.org/0000-0001-5691-1493, Highwood, E. J., Booth, B. B. B. and Carslaw, K. S. (2015) Quantifying sources of inter-model diversity in the cloud albedo effect. Geophysical Research Letters, 42 (5). pp. 1568-1575. ISSN 0094-8276 doi: 10.1002/2015GL063301 Available at https://centaur.reading.ac.uk/39368/

It is advisable to refer to the publisher's version if you intend to cite from the work. See Guidance on citing.

Published version at: http://onlinelibrary.wiley.com/doi/10.1002/2015GL063301/abstract;jsessionid=5924361694F073FFDF955C1DF4384EAC.f03t02

To link to this article DOI: http://dx.doi.org/10.1002/2015GL063301

Publisher: American Geophysical Union

All outputs in CentAUR are protected by Intellectual Property Rights law, including copyright law. Copyright and IPR is retained by the creators or other copyright holders. Terms and conditions for use of this material are defined in the End User Agreement.

www.reading.ac.uk/centaur

University of Reading

CentAUR

Central Archive at the University of Reading

Reading's research outputs online

Auxilary material for "Quantifying sources of inter-model diversity in the cloud albedo effect"

L. J. Wilcox,[1] E. J. Highwood,[2] B. B. B. Booth,[3] and K. S. Carslaw[4]

Analysis focusses on four models, where the underlying equations are known, and key variables are available in the CMIP5 archive: HadGEM2-ES, CSIRO-Mk3.6.0, IPSL-CM5A-LR, and NorESM1-M. In each of these models, the first indirect effect is represented by an equation for cloud droplet effective radius in terms of cloud droplet number concentration. Cloud droplet number concentration (N_d) is a function of either aerosol

B. B. B. Booth, Met Office Hadley Centre, FitzRoy Road, Exeter, EX1 3PB, UK. (ben.booth@metoffice.gov.uk)

K. S. Carslaw, School of Earth and Environment, University of Leeds, Leeds, LS2 9JT, UK. (K.S.Carslaw@leeds.ac.uk)

E. J. Highwood, Department of Meteorology,University of Reading, Earley Gate, P.O. Box 243, Reading, RG6 6BB, UK. (e.j.highwood@reading.ac.uk)

L. J. Wilcox, National Centre for Atmospheric Science (Climate), Department of Meteorology, University of Reading, Earley Gate, P.O. Box 243, Reading, RG6 6BB, UK. (l.j.wilcox@reading.ac.uk)

[1]National Centre for Atmospheric Science,

mass concentration, or aerosol number concentration. Both relationships introduce a source of inter-model diversity. Analysis of the influence of the N_d calculation has been the topic of many previous studies, some of which analyse the underlying equations of the models we consider here [*Storelvmo et al.*, 2009]. We focus on the influence of the relationship between N_d and cloud droplet effective radius.

1. Full-model and simple functional forms

We aim to create a simple functional form with which to test the sensitivity of the full climate model to perturbations of various parameters. We assume that sulfate accounts for most of the changes in effective radius over the industrial era, even though other aerosol species can act as CCN. We find a linear correlation between global-mean annual-mean vertically integrated sulfate load and N_d ($r^2 \geq 0.98$ for HadGEM2-ES, CSIRO-Mk3.6.0, and NorESM1-M; data was not available for IPSL-CM5A-LR), which allows the substitution of N_d for sulfate load in our analysis. Linear regression is then used to create a

[1]Department of Meteorology, University of Reading

[2]Department of Meteorology, University of Reading

[3]Met Office Hadley Centre

[4]School of Earth and Environment, University of Leeds

simple equation for effective radius in terms of sulfate load, where sulfate load and effective radius have the same power relationship as the aerosol-dependent term and effective radius in the full model. Constants from the regression analysis are regionally dependent due to different regional trends in cloud liquid water path. Our simple equations underestimate the interannual variability in effective radius relative to the full model output as they do not account for inter-annual variability in liquid water path.

The four models, their underlying equations, and the simple equations based on these are introduced below.

1.1. HadGEM2-ES

The Met Office Hadley Centre Global Environment Model 2 - Earth System, HadGEM2-ES, is a coupled AOGCM with an atmospheric resolution of N96 ($1.875° \times 1.875°$), and 38 vertical levels. It includes an interactive tropospheric chemistry scheme, interactive land and ocean carbon cycles, and dynamic vegetation [*Jones et al.*, 2011]. Seven aerosol species are represented in HadGEM2-ES: sulfate, fossil-fuel black and organic carbon, sea salt, mineral dust, biomass burning and biogenic aerosols [*Collins et al.*, 2008]. HadGEM2-ES accounts for both anthropogenic sources of sulphur, and natural sulphur from DMS and continuously degassing volcanoes.

Bellouin et al. [2007] give details of the updates to the aerosol scheme between HadGEM1 and HadGEM2, and their effects. Key changes introduced in HadGEM2 include improvements to the sulfate and biomass burning schemes, and the representation of new aerosol species: mineral dust and secondary organic aerosol.

The number concentration of hydrophilic aerosols is given by:

$$A = A_{SO_4} + A_f + A_j \tag{1}$$

$$A_{SO_4} = 5.125 \times 10^{17}.m \tag{2}$$

$$A_f = \begin{cases} 3.856 \times 10^6(1 - e^{-0.736u}), & 0\text{m s}^{-1} \leq u \leq 2\text{m s}^{-1} \\ 10^{(0.095u+6.283)}, & 2\text{m s}^{-1} \leq u \leq 17.5\text{m s}^{-1} \\ 1.5 \times 10^8(1 - 97.87e^{-0.313u}), & u > 17.5\text{m s}^{-1} \end{cases} \tag{3}$$

$$A_j = \begin{cases} 0.671 \times 10^6(1 - e^{-1.351u}), & 0\text{m s}^{-1} \leq u \leq 2\text{m s}^{-1} \\ 10^{(0.0422u+5.7122)}, & 2\text{m s}^{-1} \leq u \leq 17.5\text{m s}^{-1} \\ 3.6 \times 10^6(1 - 103.926e^{-0.353u}), & u > 17.5\text{m s}^{-1} \end{cases} \tag{4}$$

where A is the aerosol number concentration, A_{SO_4} is the number concentration of ammonium sulfate particles, A_f and A_j are the number concentrations of sea salt aerosol particles originating from film and jet droplets respectively, m is the total mass concentration of aerosol sulfur, and u is the 10m wind speed [*Jones et al.*, 2001].

The aerosol number concentration is used to find the cloud droplet number concentration, N_d:

$$N_d = \max\{3.75 \times 10^8(1 - e^{-2.5\times10^{-9}A}), N_{min}\} \tag{5}$$

$$N_{min} = \begin{cases} 3.5 \times 10^7 & \text{over ice-free land} \\ 5 \times 10^6 & \text{otherwise} \end{cases} \tag{6}$$

Effective radius is then found from:

$$r_e = \left(\frac{3q_c\rho_0}{4\pi\rho_w k N_d}\right)^{\frac{1}{3}} \tag{7}$$

where r_e is the cloud droplet effective radius, q_c is the cloud liquid water content, ρ_0 and ρ_w are the densities of air and water respectively, and k is a constant whose values depend on whether the clouds are over land or sea in the model [*Jones et al.*, 2001].

$$k = \begin{cases} 0.67, & \text{continental} \\ 0.80, & \text{marine} \end{cases} \tag{8}$$

Following this, the HadGEM2-ES simple equation has the form:

$$r_e = a + b.load^{-0.33} \quad (9)$$

where the global and regional values of constants a and b are found by linear least squares regression of global- and regional-mean time series of $load^{-0.33}$ onto global- and regional-mean time series of r_e. The global and regional values of the constants a and b are shown in Table 2.

1.2. CSIRO-Mk3.6.0

The Commonwealth Scientific and Industrial Research Organisation model 3.6, CSIRO-Mk3.6.0, is a coupled AOGCM with dynamical sea ice and soil canopy schemes. The atmosphere has a horizontal resolution of T63 ($\approx$1.875°$\times$1.875°), and 18 vertical levels. The main difference between CSIRO-Mk3.6.0 and Mk3.5 is the inclusion of an interactive aerosol scheme. This explicitly treats sulfate, carbonaceous aerosol, dust, and sea salt. Mk3.6 also includes an updated radiation scheme, and other changes to the atmospheric physics component [*Syktus et al.*, 2011].

Prescribed anthropogenic and biomass burning sources of sulfur, black carbon, and organic aerosol are based on *Lamarque et al.* [2010], but with emissions of black carbon and organic aerosol uniformly increased by 25% and 50% respectively in order to improve the agreement between modelled and observed carbonaceous aerosol. Natural sources of sulfur are continuously degassing volcanoes, and biogenic emissions of DMS [*Rotstayn et al.*, 2012].

Rotstayn et al. [2012] note that CSIRO-Mk3.6.0 burdens of sulfate, organic aerosol, and dust in 2000 are close to the top of their reference range. The relatively large sulfate

burdens can be seen in Supplementary Figures 3 and 4. *Rotstayn et al.* [2012] find that large DMS emissions are a contributing factor to the relatively large sulfate burden in the model.

The number concentration of hydrophilic aerosol is given by:

$$A = A_S + A_{SS} + A_C \tag{10}$$

$$A_S = 5.1 \times 10^{17} m_S \tag{11}$$

$$A_C = 3.0 \times 10^{17} m_C \tag{12}$$

where A is the number concentration of hydrophilic aerosols, A_S is the sulfate concentration, A_{SS} is the sea salt concentration, A_C is the concentration of hydrophilic carbonaceous aerosol, and m_S and m_C are the mass concentrations of sulfate and hydrophilic carbonaceous aerosol respectively. A_{SS} is provided directly by the windspeed-dependent diagnostic for sea salt [*Rotstayn et al.*, 2012].

Cloud droplet number concentration, N_d, is given by:

$$N_d = max\{3.75 \times 10^8 (1 - e^{-2.5 \times 10^{-9} A}), N_{min}\} \tag{13}$$

$$N_{min} = 10 \times 10^6 \tag{14}$$

The calculation of cloud droplet effective radius includes a parameterization of increased droplet dispersion with increased cloud droplet number concentration, such that:

$$r_e = 0.07 r_v \left(\frac{L}{N}\right)^{-1.14} \tag{15}$$

$$r_v = \left(\frac{3 L \rho_0}{4\pi \rho_w N_d}\right)^{\frac{1}{3}} \tag{16}$$

$$r_e = 0.07 \left(\frac{3\rho_0}{4\pi\rho_w}\right)^{\frac{1}{3}} \left(\frac{L}{N_d}\right)^{0.19} \tag{17}$$

where L is the cloud liquid water content, r_v is the volume-averaged mean droplet radius, and ρ_0 and ρ_w are the densities of air and water respectively [*Rotstayn et al.*, 2012].

Following this, the CSIRO-Mk3.6.0 simple equation has the form:

$$r_e = a + b.load^{-0.19} \tag{18}$$

where the global and regional values of constants a and b are found by linear least squares regression of global- and regional-mean time series of $load^{-0.19}$ onto global- and regional-mean time series of r_e. The global and regional values of the constants a and b are shown in Table 2.

1.3. IPSL-CM5A-LR

The Institut Pierre Simon Laplace Climate Model 5A (low resolution), IPSL-CM5A-LR, is an AOGCM with an interactive carbon cycle, representation of tropospheric and stratospheric chemistry, and a comprehensive representation of aerosol processes [*Dufresne et al.*, 2013]. It has a horizontal resolution of $3.75° \times 1.875°$, and 39 vertical levels. IPSL-CM5A-LR treats sulfate, black carbon, particulate organic matter, sea salt, and dust. The model represents a substantial improvement over its predecessor, which only considered sulfate aerosol [*Dufresne et al.*, 2013].

The total mass of soluble aerosol is given by:

$$m_{soluble} = m_{SO_4} + m_{BC,soluble} + m_{POM,soluble} \tag{19}$$

where m_{SO_4}, $m_{BC,soluble}$, and $m_{POM,soluble}$ are the masses of sulfate, soluble black carbon, and soluble particulate organic matter respectively [*Szopa et al.*, 2012].

Cloud droplet number concentration, N_d, is given by:

$$N_d = 10^{1.7+0.2\log(m_{soluble})} \tag{20}$$

Effective radius is then found from:

$$r_e = 1.1\left(\frac{L\rho_{air}}{\frac{4}{3}\pi\rho_{water}N_d}\right)^{\frac{1}{3}} \tag{21}$$

where r_e is the cloud droplet effective radius, L is the cloud liquid water content, and ρ_{air} and ρ_{water} are the densities of air and water respectively [*Boucher and Lohmann*, 1995].

The IPSL-CM5A-LR simple equation has the form:

$$r_e = a + b.load^{-0.33} \tag{22}$$

where the global and regional values of constants a and b are found by linear least squares regression of global- and regional-mean time series of $load^{-0.33}$ onto global- and regional-mean time series of r_e. The global and regional values of the constants a and b are shown in Table 2.

1.4. NorESM1-M

The Norwegian Earth System Model, NorESM1-M, is based on CCSM4 (Community Climate System Model version 4). It's atmospheric component is CAM4-Oslo, a modified version of CAM4 (Community Atmosphere Model 4), which includes advanced chemistry-aerosol-cloud-radiation interactions [*Bentsen et al.*, 2013]. It has a horizontal resolution of 2.5°×1.9°, and 26 vertical levels.

NorESM1-M includes sea salt, mineral dust, particulate sulfate, black carbon, and primary and secondary organic aerosols [*Kirkevåg et al.*, 2013]. Key updates from the previous version of the model include: modified prognostic sea salt emissions; updated

treatment of precipitation scavenging and gravitational settling; increased abundance of organic matter relative to black carbon; and the inclusion of biogenic primary organic and methanesulfonic acid from the oceans [*Kirkevåg et al.*, 2013].

The activation of CCN in NorESM1-M follows the parameterization of *Abdul-Razzak and Ghan* [2000] [*Kirkevåg et al.*, 2013]. In an update over the previous version, cloud droplet spectral dispersion is represented, so that:

$$r_e = \beta r_v \tag{23}$$

$$r_v = \left(\frac{3L\rho_0}{4\pi\rho_w N_d}\right)^{\frac{1}{3}} \tag{24}$$

$$\beta = \frac{(1+2\epsilon^2)^{\frac{2}{3}}}{(1+\epsilon^2)^{\frac{1}{3}}} \tag{25}$$

$$\epsilon = 1 - 0.7e^{-0.003N_d} \tag{26}$$

$$r_e = \left(\frac{3L\rho_{air}}{4\pi\rho_w N_d}\right)^{\frac{1}{3}} \frac{(1+2\epsilon^2)^{\frac{2}{3}}}{(1+\epsilon^2)^{\frac{1}{3}}} \tag{27}$$

Following this, the NorESM1-M simple equation is more complex than that for the other models we consider:

$$r_e = a + b.load^{-0.33} \frac{(1+2(1-0.7e^{3000load})^2)^{0.66}}{(1+(1-0.7e^{3000load})^2)^{0.33}} \tag{28}$$

where the global and regional values of constants a and b are found by linear least squares regression of global- and regional-mean time series of:

$$load^{-0.33} \frac{(1+2(1-0.7e^{3000load})^2)^{0.66}}{(1+(1-0.7e^{3000load})^2)^{0.33}} \tag{29}$$

onto global- and regional-mean time series of r_e. The global and regional values of the constants a and b are shown in Table 2.

References

Abdul-Razzak, H., and S. J. Ghan (2000), A parameterization of aerosol activation: 2. multiple aerosol types, *Journal of Geophysical Research: Atmospheres (1984–2012)*, *105*(D5), 6837–6844.

Bellouin, N., O. Boucher, J. Haywood, C. Johnson, A. Jones, J. Rae, and S. Woodward (2007), Improved representation of aerosols for HadGEM2, *Hadley Centre Technical Note*, *73*.

Bentsen, M., I. Bethke, J. Debernard, T. Iversen, A. Kirkevåg, Ø. Seland, H. Drange, C. Roelandt, I. Seierstad, C. Hoose, et al. (2013), The Norwegian Earth System Model, NorESM1-M-Part 1: Description and basic evaluation of the physical climate, *Geoscientific Model Development*, *6*, 687–720.

Boucher, O., and U. Lohmann (1995), The sulfate-CCN-cloud albedo effect, *Tellus B*, *47*(3), 281–300.

Collins, W., N. Bellouin, M. Doutriaux-Boucher, N. Gedney, T. Hinton, C. Jones, S. Liddicoat, G. Martin, F. O'Connor, J. Rae, et al. (2008), Evaluation of the HadGEM2 model, *Hadley Cent. Tech. Note*, *74*.

Collins, W., N. Bellouin, M. Doutriaux-Boucher, N. Gedney, P. Halloran, T. Hinton, J. Hughes, C. Jones, M. Joshi, S. Liddicoat, et al. (2011), Development and evaluation of an Earth-system model–HadGEM2, *Geosci. Model Dev.*, *4*(4), 1051–1075.

Donner, L., B. Wyman, R. Hemler, L. Horowitz, Y. Ming, M. Zhao, J. Golaz, P. Ginoux, S. Lin, M. Schwarzkopf, et al. (2011), The dynamical core, physical parameterizations, and basic simulation characteristics of the atmospheric component AM3 of the GFDL

global coupled model CM3, *Journal of Climate*, *24*(13), 3484–3519.

Dufresne, J.-L., M.-A. Foujols, S. Denvil, A. Caubel, O. Marti, O. Aumont, Y. Balkanski, S. Bekki, H. Bellenger, R. Benshila, et al. (2013), Climate change projections using the IPSL-CM5 Earth System Model: from CMIP3 to CMIP5, *Climate Dynamics*, *40*(9-10), 2123–2165.

Iversen, T., M. Bentsen, I. Bethke, J. Debernard, A. Kirkevåg, Ø. Seland, H. Drange, J. Kristjánsson, I. Medhaug, M. Sand, et al. (2012), The Norwegian Earth System Model, NorESM1-M–part 2: Climate response and scenario projections, *Geoscientific Model Development Discussions*, *5*, 2933–2998.

Jones, A., D. L. Roberts, M. J. Woodage, and C. E. Johnson (2001), Indirect sulphate aerosol forcing in a climate model with an interactive sulphur cycle, *Journal of Geophysical Research: Atmospheres (1984–2012)*, *106*(D17), 20,293–20,310.

Jones, C., J. Hughes, N. Bellouin, S. Hardiman, G. Jones, J. Knight, S. Liddicoat, F. O'Connor, R. J. Andres, C. Bell, et al. (2011), The HadGEM2-ES implementation of CMIP5 centennial simulations, *Geoscientific Model Development*, *4*(3), 543–570.

Kirkevåg, A., T. Iversen, Ø. Seland, C. Hoose, J. Kristjánsson, H. Struthers, A. M. Ekman, S. Ghan, J. Griesfeller, E. D. Nilsson, et al. (2013), Aerosol–climate interactions in the Norwegian Earth System Model–NorESM1-M, *Geoscientific Model Development*, *6*(1), 207–244.

Lamarque, J., T. Bond, V. Eyring, C. Granier, A. Heil, Z. Klimont, D. Lee, C. Liousse, A. Mieville, B. Owen, et al. (2010), Historical (1850-2000) gridded anthropogenic and biomass burning emissions of reactive gases and aerosols: methodology and application,

Atmospheric Chemistry and Physics, *10*(15), 7017–7039.

Levy, H., L. W. Horowitz, M. D. Schwarzkopf, Y. Ming, J. C. Golaz, V. Naik, and V. Ramaswamy (2013), The Roles of Aerosol Direct and Indirect Effects in Past and Future Climate Change, *Journal of Geophysical Research: Atmospheres*, *118*(10), 4521–4532.

Rotstayn, L., S. Jeffrey, M. Collier, S. Dravitzki, A. Hirst, J. Syktus, and K. Wong (2012), Aerosol-and greenhouse gas-induced changes in summer rainfall and circulation in the Australasian region: a study using single-forcing climate simulations, *Atmospheric Chemistry & Physics*, *12*, 6377–6404.

Storelvmo, T., U. Lohmann, and R. Bennartz (2009), What governs the spread in shortwave forcings in the transient IPCC AR4 models?, *Geophysical Research Letters*, *36*(1).

Syktus, J., S. Jeffrey, et al. (2011), The CSIRO-QCCCE contribution to CMIP5 using the CSIRO Mk3.6 climate model, in *MODSIM2011, 19th International Congress on Modelling and Simulation. Modelling and Simulation Society of Australia and New Zealand*, pp. 2782–88.

Szopa, S., Y. Balkanski, M. Schulz, S. Bekki, D. Cugnet, A. Fortems-Cheiney, S. Turquety, A. Cozic, C. Déandreis, D. Hauglustaine, et al. (2012), Aerosol and ozone changes as forcing for climate evolution between 1850 and 2100, *Climate Dynamics*, pp. 1–28.

Voldoire, A., E. Sanchez-Gomez, D. Salas y Mélia, B. Decharme, C. Cassou, S. Sénési, S. Valcke, I. Beau, A. Alias, M. Chevallier, et al. (2012), The CNRM-CM5. 1 global climate model: description and basic evaluation, *Climate Dynamics*, pp. 1–31.

von Salzen, K., J. Scinocca, N. McFarlane, J. Li, J. Cole, D. Plummer, D. Verseghy, M. Reader, X. Ma, M. Lazare, et al. (2013), The Canadian fourth generation Atmospheric Global Climate Model (CanAM4). Part I: Representation of physical processes, *Atmosphere-Ocean*, (ahead-of-print), 1–22.

Watanabe, M., T. Suzuki, R. O'ishi, Y. Komuro, S. Watanabe, S. Emori, T. Takemura, M. Chikira, T. Ogura, M. Sekiguchi, et al. (2010), Improved climate simulation by MIROC5: Mean states, variability, and climate sensitivity, *Journal of Climate*, *23*(23), 6312–6335.

Watanabe, S., T. Hajima, K. Sudo, T. Nagashima, T. Takemura, H. Okajima, T. Nozawa, H. Kawase, M. Abe, T. Yokohata, et al. (2011), MIROC-ESM: model description and basic results of CMIP5-20c3m experiments, *Geoscientific Model Development Discussions, Volume 4, Issue 2, 2011, pp. 1063-1128*, *4*, 1063–1128.

Yukimoto, S., Y. Adachi, and M. Hosaka (2012), A new Global Climate Model of the Meteorological Research Institute: MRI-CGCM3: Model description and basic performance (special issue on recent development on climate models and future climate projections), *Journal of the Meteorological Society of Japan*, *90*, 23–64.

Table 1. CMIP5 models used in this study.

Institute	Model	1^{st} Indirect	2^{nd} Indirect	Ant	Reference
CCCma	CanESM2	Y	N	E1	*von Salzen et al.* [2013]
CNRM-CERFACS	CNRM-CM5	Y	N	E1	*Szopa et al.* [2012]
					Voldoire et al. [2012]
CSIRO-QCCCE	**CSIRO-Mk3.6.0**	Y	Y	E1a	*Rotstayn et al.* [2012]
NOAA GFDL	GFDL-CM3	Y	Y	E1	*Donner et al.* [2011]
					Levy et al. [2013]
MOHC	HadGEM2-CC	Y	Y	E1	*Bellouin et al.* [2007]
					Collins et al. [2011]
MOHC	**HadGEM2-ES**	Y	Y	E1	*Bellouin et al.* [2007]
					Collins et al. [2011]
IPSL	**IPSL-CM5A-LR**	Y	N	E1	*Dufresne et al.* [2013]
IPSL	IPSL-CM5A-MR	Y	N	E1	*Dufresne et al.* [2013]
NCC	**NorESM1-M**	Y	Y	E1	*Iversen et al.* [2012]
MIROC	MIROC5	Y	Y	E1	*Watanabe et al.* [2010]
MIROC	MIROC-ESM	Y	Y	E1	*Watanabe et al.* [2011]
MIROC	MIROC-ESM-CHEM	Y	Y	E1	*Watanabe et al.* [2011]
MRI	MRI-CGCM3	Y	N	E1	*Yukimoto et al.* [2012]
					Pers. Comm., S. Yukimoto [2013]

Table 2. Values of the constants in the simple equations for cloud droplet effective radius in terms of vertically integrated sulfate load.

	HadGEM2-ES		CSIRO-Mk3.6.0		IPSL-CM5A-LR		NorESM1-M	
	a($\times 10^{-6}$)	b($\times 10^{-8}$)	a($\times 10^{-6}$)	b($\times 10^{-7}$)	a($\times 10^{-7}$)	b($\times 10^{-9}$)	a($\times 10^{-6}$)	b($\times 10^{-8}$)
Globe	9.24	2.73	8.11	2.32	21.6	4.70	10.1	1.12
Europe	5.15	5.70	6.96	2.62	7.86	2.28	9.01	3.48
N. Atlantic	7.66	4.14	7.96	2.00	28.8	10.1	10.4	1.24
China	6.28	3.85	6.68	3.15	8.80	4.41	8.62	3.82
US	6.57	2.28	8.86	0.45	6.04	1.93	10.1	1.49

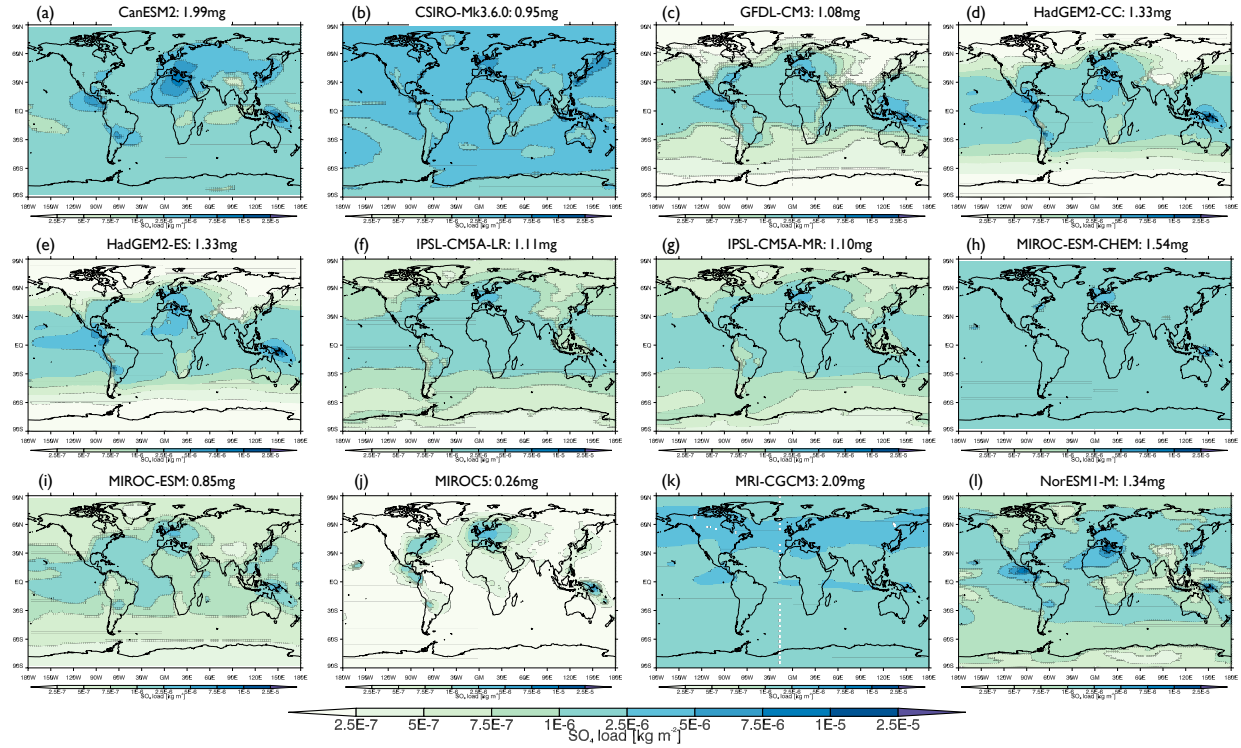

Figure 1. 1860-1900 column total sulfate load for (a): CanESM2, (b): CSIRO-Mk3.6.0, (c): GFDL-CM3, (d): HadGEM2-CC, (e): HadGEM2-ES, (f): IPSL-CM5A-LR, (g): IPSL-CM5A-MR, (i): MIROC-ESM-CHEM, (j): MIROC-ESM, (k): MIROC5, (l): MRI-CGCM3, (m): NorESM1-M.

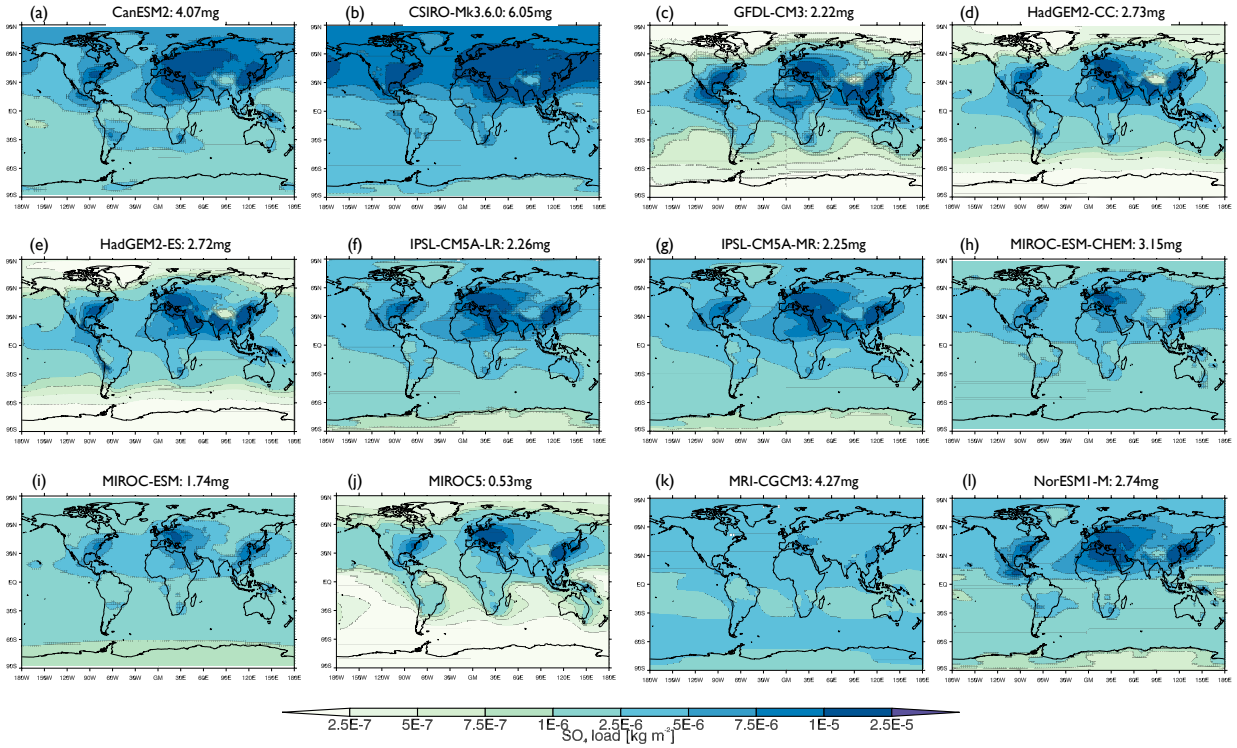

Figure 2. 1986-2005 mean column total sulfate load for (a): CanESM2, (b): CSIRO-Mk3.6.0, (c): GFDL-CM3, (d): HadGEM2-CC, (e): HadGEM2-ES, (f): IPSL-CM5A-LR, (g): IPSL-CM5A-MR, (i): MIROC-ESM-CHEM, (j): MIROC-ESM, (k): MIROC5, (l): MRI-CGCM3, (m): NorESM1-M.

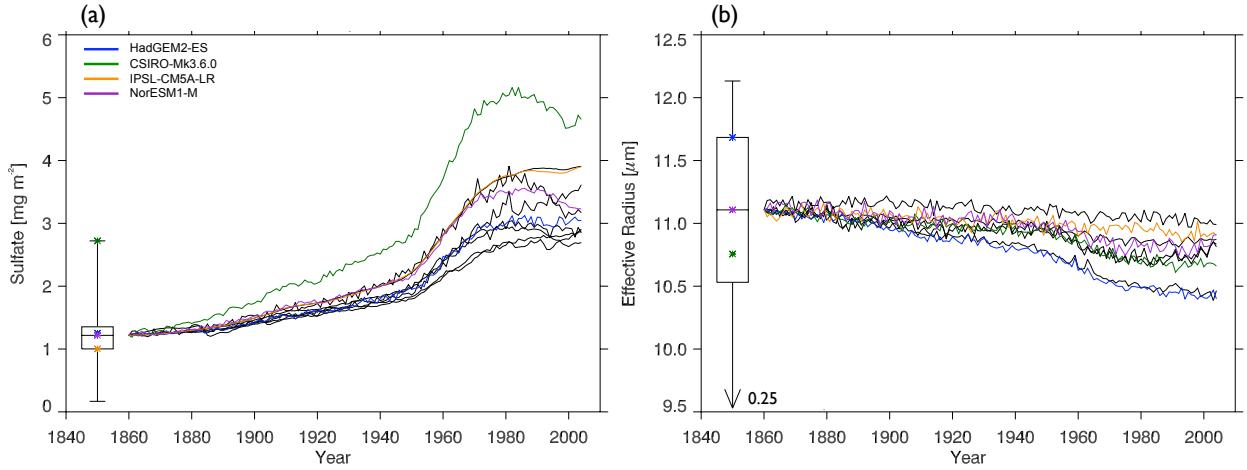

Figure 3. Annual-mean global-mean (a): sulfate load and (b): cloud-top effective radius for CMIP5 models. Time series are adjusted to the 1860 CMIP5 median value. The box and whisker shows median, interquartile range, and absolute range. Colours pick out the models focussed on in this study. Crosses show the location of these models within the CMIP5 range.

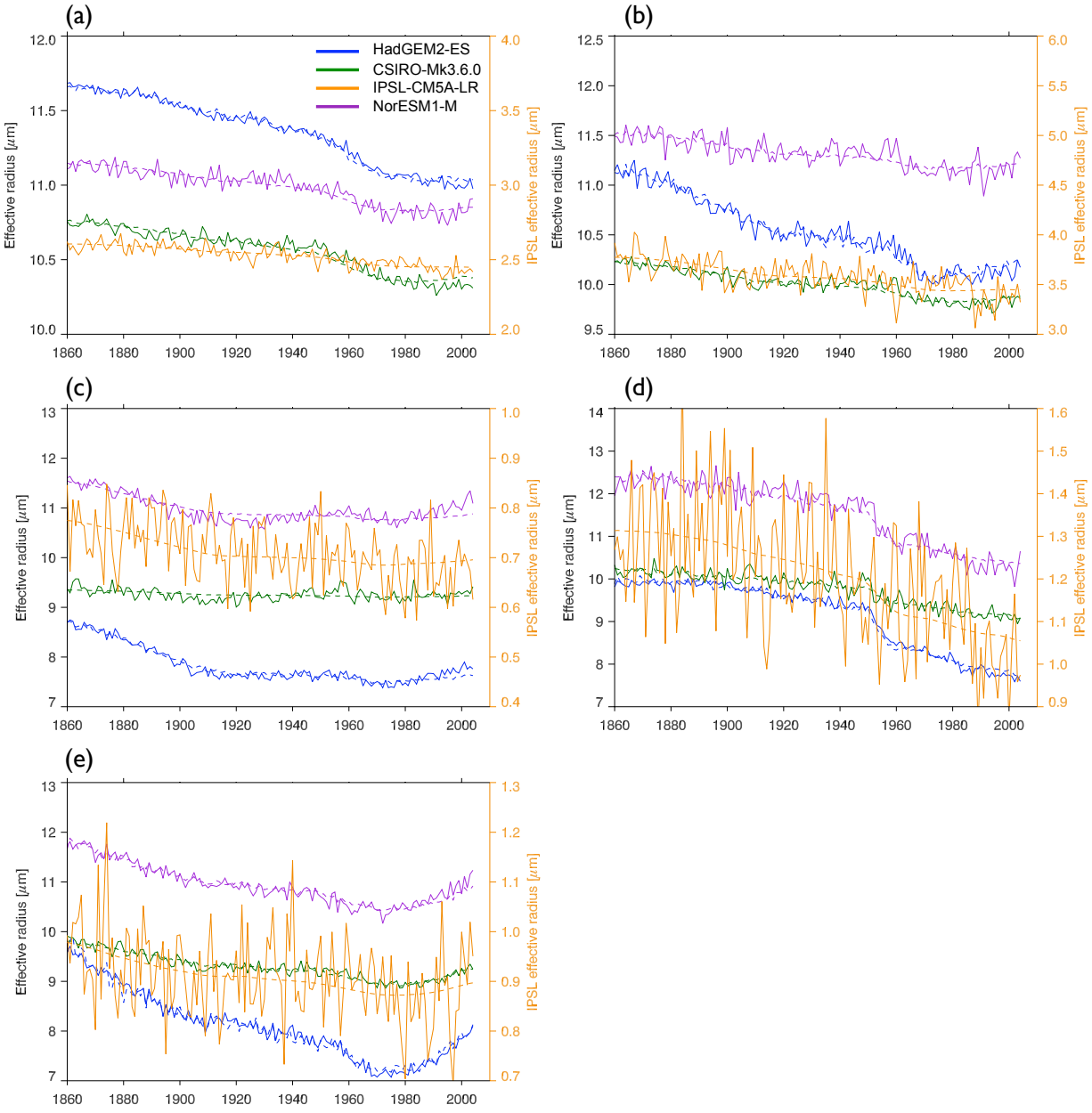

Figure 4. Annual-mean cloud-top effective radius output from CMIP5 models (solid lines), and produced using simplified equations in terms of sulfate load (dotted lines) for (a): Global, (b): China, (c): Europe, (d): North Atlantic, (e): continental United States mean. Note that all results for IPSL-CM5A-LR are shown on a separate axis.

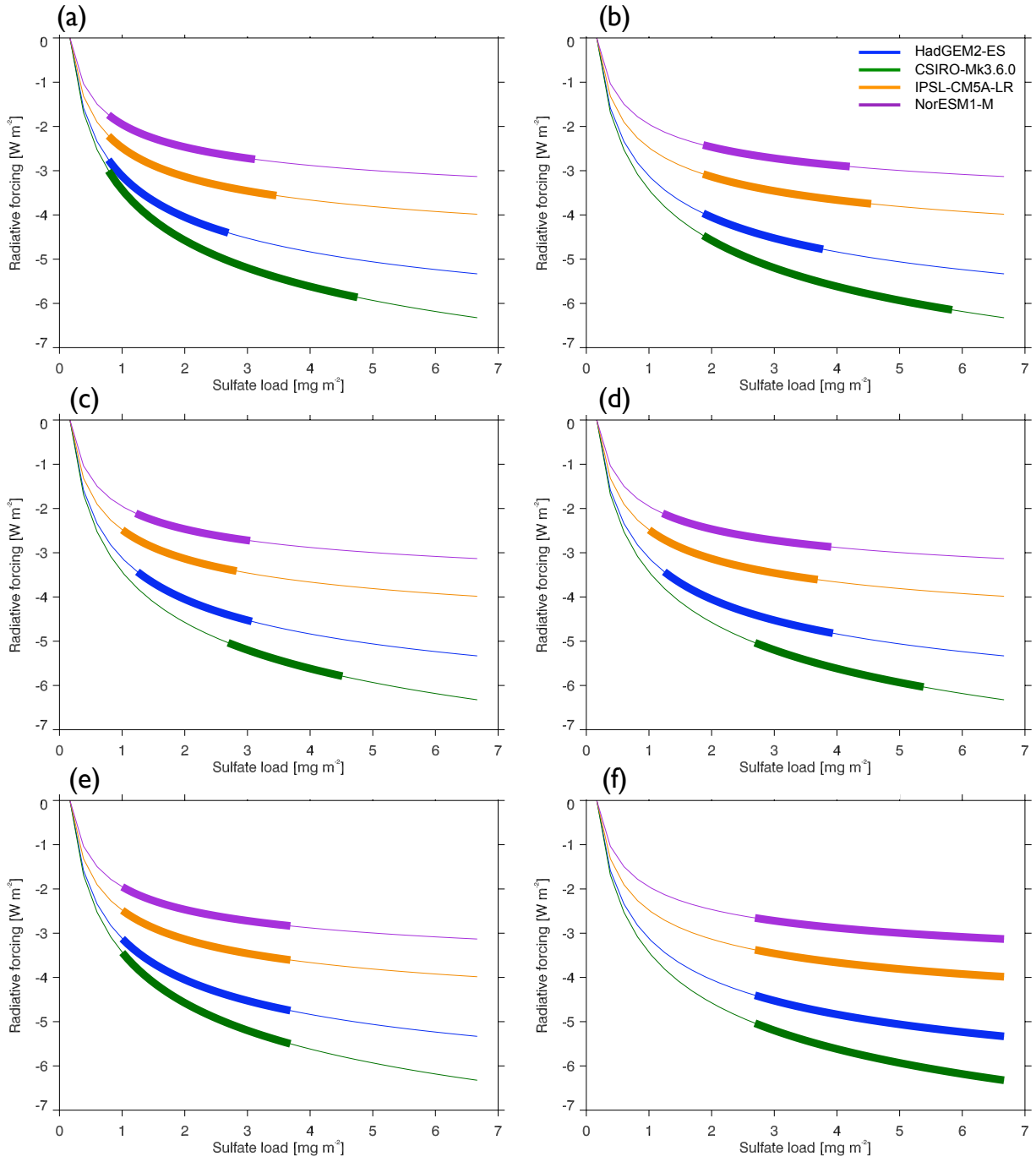

Figure 5. Schematic showing the perturbations to sulfate load made in the sensitivity experiments, and their impact on radiative forcing. Thin lines use the functional forms to show cloud albedo for the whole CMIP5 range of global mean sulfate load. Thick lines highlight the sulfate loads used in each model in each experiment. (a): Minimum pre-industrial load, (b): maximum pre-industrial load, (c): minimum load change, (d): maximum load change, (e): IPSL-CM5A-LR load, (f): CSIRO-Mk3.6.0 load.